

TRANSPORT, MAGNETIC AND THERMAL PROPERTIES OF $(\text{Fe}_{100-x}\text{V}_x)_{75}\text{P}_{15}\text{C}_{10}$ SEMI-AMORPHOUS RIBBONS

*M.A.S. KARAL, M. KAMRUZZAMAN, M.G.M. HOSSAIN, H.M.I. JAIM¹ and F.A. KHAN

Department of Physics, Bangladesh University of Engineering and Technology, Dhaka-1000, Bangladesh

¹Department of Mechanical Engineering, Bangladesh University of Engineering and Technology, Dhaka-1000, Bangladesh

(Received January 21, 2011 and accepted in revised form March 14, 2011)

$(\text{Fe}_{100-x}\text{V}_x)_{75}\text{P}_{15}\text{C}_{10}$ [$x=1.5, 3, 9$ and 15] semi-amorphous alloys (partially crystalline) in the form of ribbon were prepared by the standard melt spinning technique and studied their transport, magnetic and thermal properties. The nature of the as prepared samples was studied by x-ray diffraction (XRD). The resistivity of the samples was investigated from temperature 93K to 800 K. The resistivity followed 'Mooij Correlation' at low temperature (93 K-300 K). The resistivity at higher temperature (300 K-800 K) remained constant upto a certain temperature and then decreased with temperature rise. The Hall resistivity and the magnetoresistance (MR) were measured in an applied magnetic field upto 0.6 T at room temperature (RT=300 K). Anomalous Hall effect was observed in the Hall resistivity measurement and MR was found to vary 0-8%. The saturation magnetization gradually decreases with the increase of the substitution of Fe by V at RT. Both the impedance magnitude and phase angle remained constant upto 10^6 Hz and then remarkably increased with frequency. The thermal properties associated with crystallization temperature and weight changes were measured by using the differential thermal analyzer (DTA) and the thermo gravimetric (TG) techniques respectively.

Keywords : XRD, Resistivity, Hall resistivity, MR, Magnetization, Impedance, DTA.

1. Introduction

For the last few decades metallic glasses were studied extensively due to their unique mechanical, thermal and magnetic properties [1-4]. Iron-based glassy alloys have been used in many electrical devices such as magnetic wires, sensors, band-pass filters, magnetic shielding and energy-saving electric power transformers [5-7] due to their satisfactory soft magnetic properties. Isotropic and anisotropic spin scattering mechanism should contribute to the resistivity and anomalous Hall effect in magnetically ordered amorphous metals [8-11]. For the scattering centers magnons, magnetic impurities and topological spin disorder had been proposed [8, 11, 12]. In many cases, the structural disorder of the atomic sites was projected onto the spin lattice [9, 13] thus introducing a magnetic scattering contribution to the resistivity aside from thermal excitations. However, this contribution was found to be small in most cases [9, 11, 14]; apparently, anisotropic scattering was a sensitive tool to identify spin scattering contributions in amorphous metals

[8, 12, 15]. Mooij [16] pointed out a correlation of the electrical resistivity (ρ) and its temperature coefficient of resistivity ($\text{TCR}=1/\rho \times d\rho/dT$) at low temperature in metallic alloys. Mooij observed that TCR changes sign in a relatively narrow range of resistivity (i. e., the critical resistivity for which $\text{TCR}=0$, $\rho_c \approx 100\text{-}160 \mu\Omega\text{-cm}$). For $\rho > 160 \mu\Omega\text{-cm}$, the ρ usually decreases as temperature T increases, in contrast to the normal metallic behavior seen for lower ρ systems. Most theoretical approaches to the Mooij correlation are based on quantum-mechanical coherence effects, namely, the incipient Anderson localization [17]. It has been argued that the breakdown of the adiabatic approximation, leads to phonon-assisted tunneling and, therefore, to a negative TCR. The magnetic properties of the transition elements are critically dependent on fine details of the electronic structure of the d-electrons.

Within Stoner's model for ferromagnetism [18], the effective moment of an iron atom in metallic iron and in iron alloys is mainly due to the effective spins of the 3d electrons. In general the orbital

* Corresponding author : asayem221@phy.buet.ac.bd

moment of iron atoms is strongly quenched by the electric field. Alloying Fe with 3d elements affects the magnetic moments and also the saturation magnetization [19-22]. Although there was a wide consensus about this decrease theoretically [23-26], the question has not been investigated in full detail experimentally. In the magnetically diluted metallic systems the atomic moments are magnetically coupled via the RKKY (Ruderman, Kittel, Kasuya and Yosida) [27] type exchange interaction and ordered into a ferromagnetic domain structure for sufficiently low temperatures. The change of magneto impedance had been investigated as high as 360% in a series of Co and Fe based amorphous ribbons [28]. The influence of stress on magneto impedance had been studied in Co based amorphous ribbons [29] and the thermal and magnetic properties had been also studied in Fe based metallic alloys [30]. DTA technique is the most frequently used method to study the crystallization behavior. However, the reaction needs to occur with a relatively large heat of crystallization and is not very useful when the reaction rate is slow or if only a small amount of heat transfer is involved. The crystallization behavior of metallic glasses has been extensively studied [31, 32]. In this study, the results are being presented on the transport, magnetic and thermal behavior of a series of as prepared $(\text{Fe}_{100-x}\text{V}_x)_{75}\text{P}_{15}\text{C}_{10}$ [$x=1.5, 3, 9$ and 15] alloys in details.

2. Experimental

2.1. XRD and EDX Measurement

The $(\text{Fe}_{100-x}\text{V}_x)_{75}\text{P}_{15}\text{C}_{10}$ [$x = 1.5, 3, 9, 15$] semi-amorphous metallic ribbons were prepared from appropriate ratio of pure elements (Fe=99.95%, V=99.95%, P=99.95% and C=99.95%) by the standard melt spinning technique [33] with wheel speed of 25 m/s and cooling rate 1.8×10^6 °C/min. The ribbons used for measurements had a width of 1 mm, a thickness of 25 μm and a length of 2-20 cm. The amorphous nature of the as prepared samples was checked by XRD (Model: X'Pert PRO XRD PW 3040 Phillips) with $\text{CuK}\alpha$ radiation ($\lambda=1.54178$ Å). The 2θ values were carried out from 30° to 65°. The compositions existing in the samples were measured by EDX (Model: Hitachi S-3400N EDX) at RT.

2.2. Resistivity Measurement

The resistivity of the rectangular strip size samples was measured by conventional four point

probe technique at low temperature (93 K-300 K) in a liquid nitrogen atmosphere and at higher temperature (300 K-800 K) using an oven. The Hall resistivity was measured using a conventional Hall geometry where the magnetic field applied to the perpendicular of the ribbon surface. A constant-current power supply (Model: Hewlett-Packard 6177C) and a digital nano-voltmeter (Model: Keithley 181) alongwith chromel constantan thermocouple were used in the measurement setup. When the resistance of a material changes with the applied magnetic field then the material is said to have the MR. MR usually expressed in percentage and is calculated by the following way.

$$\text{MR}\% = \frac{R(B) - R(0)}{R(0)} \times 100\%$$

Where, $R(B)$ is the resistance in presence of magnetic field and $R(0)$ is the resistance in absence of magnetic field.

2.3. Magnetization Measurement

The magnetization was measured using a vibrating sample magnetometer (VSM) at RT and a magnetic field from 0 to 1.172 kG, as described in detail elsewhere [34].

2.4. Impedance Measurement

The ac impedance magnitude and phase angle measurements were obtained using an impedance analyzer (Model: Agilent 4291B RF) making a capacitive coupling to the sample.

2.5. DTA and TG Measurement

The crystallization temperatures of the samples were monitored by a differential thermal analyzer [Model: Seiko-Ex-STAR-6300, Japan]. The measurements using DTA and TG were carried out from 40 to 850 °C at a heating rate of 20 °C min^{-1} . The DTA traces give the crystallization temperature and TG provides the weight change with temperature.

3. Results and Discussion

3.1. XRD and EDX

Fig. 1 shows the XRD pattern of the as prepared samples of $(\text{Fe}_{100-x}\text{V}_x)_{75}\text{P}_{15}\text{C}_{10}$ [$x=1.5, 3, 9$ and 15] alloys. We have seen that each sample contains a broad peak with minor crystalline peaks which confirms the samples are semi-amorphous

in nature. Fig. 2 (a-d) shows the EDX spectrum that consisting of different peaks for compositions of Fe, V, P and C. From these figures we have seen that the intensity of the Fe peak at around 1 keV gradually decreases with the increase of V content. On the other hand, the intensity of the V peak at around 5 keV gradually increases with the increase of V content of the samples. The EDX technique gives the information of the elements (but not for light elements) and their compositions.

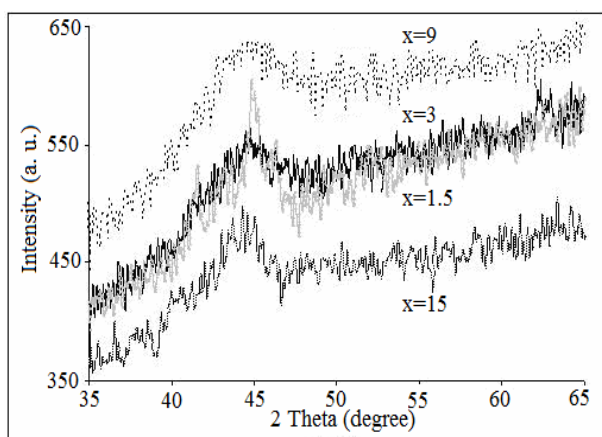


Figure 1. XRD of as prepared samples .

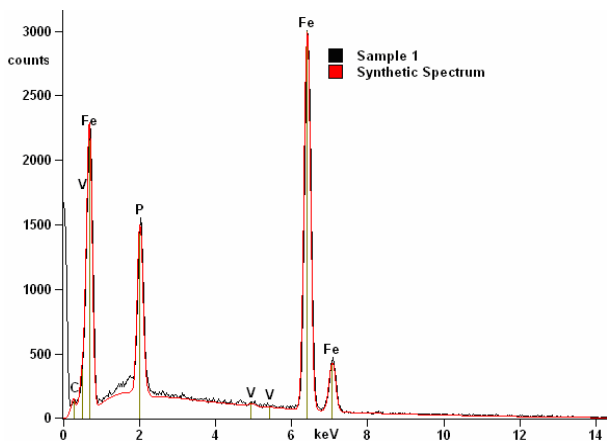


Figure 2 (a). EDX spectrum for x=1.5 .

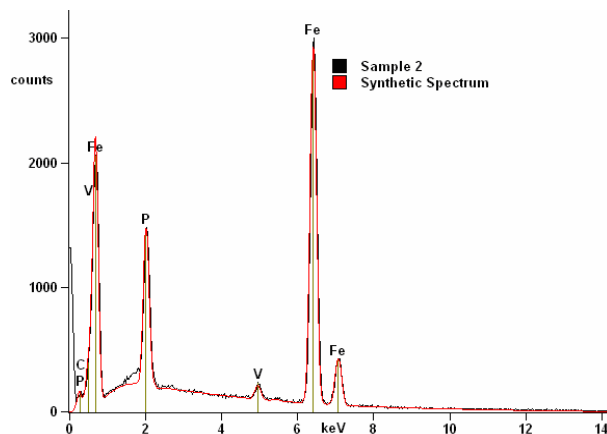


Figure 2(b). EDX spectrum for x=3 .

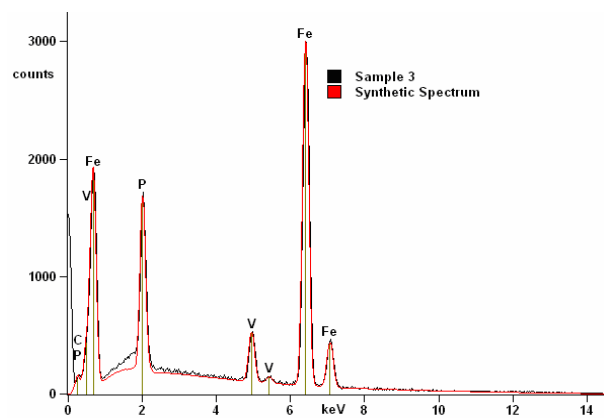


Figure 2(c). EDX spectrum for x=9 .

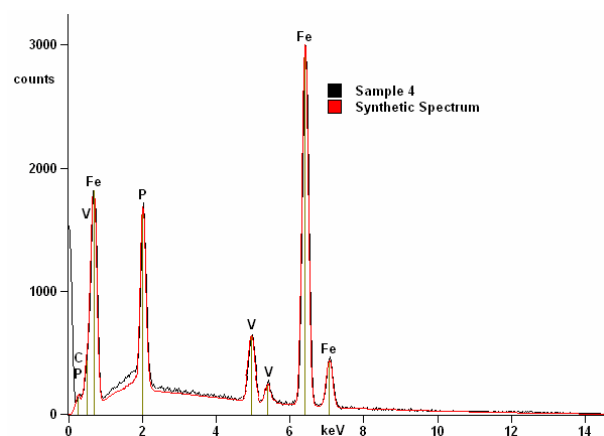


Figure 2(d). EDX spectrum for x=15 .

3.2. Resistivity

Fig. 3(a) shows the temperature dependent of normalized resistivity of the samples. The normalized resistivity decreases with the decrease in temperature for samples $x=1.5$ and 3 that may be happening due to the decrease of incoherent electron-magnon scattering. For samples $x=9$ and 15 the normalized resistivity increases with the decrease in temperature due to the structural topological scattering. For the samples $x=1.5$ and 3 the measured ρ at RT were $149 \mu\Omega\text{-cm}$ and $157 \mu\Omega\text{-cm}$ respectively that shows positive TCR. On the other hand, for the samples $x=9$ and 15 the measured ρ at RT were $182 \mu\Omega\text{-cm}$ and $206 \mu\Omega\text{-cm}$ respectively that shows negative TCR. These results follow the Mooij-correlation of metallic glasses which was based on quantum mechanical coherence effects, namely incipient Anderson localization. Such transport phenomena deviates from the conventional Boltzmann's transport. In the case of disorder metals, the wavelength of the conduction electron is comparable with the atomic distances which result in interference between scattering waves. The negative TCR is the result of reduction of interferences with temperature rises. Again, the gradual change from positive TCR to negative TCR with V content is accompanied by shortening of the mean free path down to an average atomic distance. An increase in ρ in this regime is due entirely to the mean free path effect and is free from the band structure effect.

Fig. 3(b) shows the resistivity as a function of temperature. We have observed that the resistivity remains constant upto 680 K, 710 K, 715 K and 730K for $x=1.5, 3, 9$ and 15 respectively and then decreases sharply with the increase of temperature. The decrease in resistivity corresponds to the onset of micro-crystallites formation. The process continues upto the crystallization temperature where the resistivity shows a sharp fall and the more ordered crystalline structures are expected to have formed around this temperature. These temperatures also correspond well to the crystallization temperature in the DTA measurement. The transition temperature increases with the increase of V content into the samples.

Fig. 4 shows the Hall resistivity as a function of magnetic field upto 0.6 T at RT. The Hall resistivity has shown sharp increase initially with magnetic

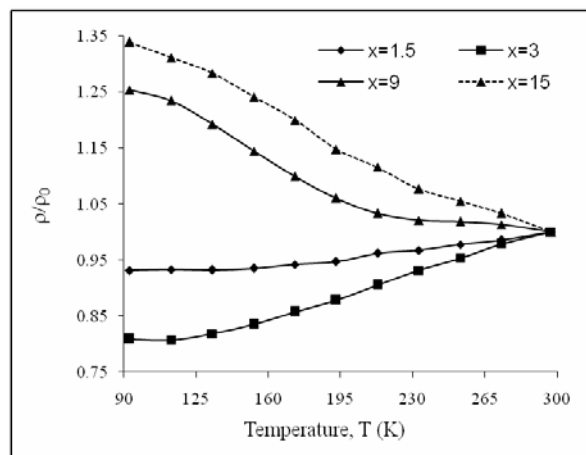


Figure 3 (a). Normalized resistivity as a function of temperature.

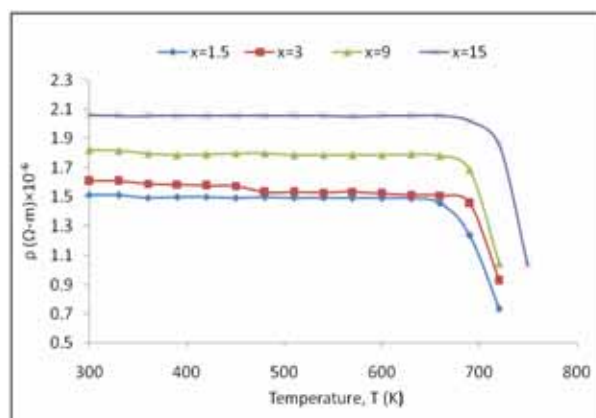


Figure 3(b). Resistivity as a function of temperature.

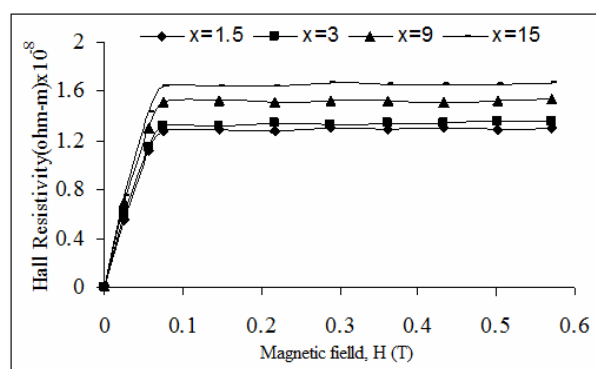


Figure 4. Hall resistivity as a function of magnetic field.

field. Once saturation is achieved, there is no domain motion as it has assumed a single domain. Hall resistivity increases with increase of V content and also the applied magnetic field. If we increase

the V content, magnetic impurities and topological spin disorder increases which may be responsible for the increase of Hall resistivity. Generally, the anomalous Hall effect results from anisotropic scattering and this in turn comes from an interplay of internal polarization, (spin) scattering centers and spin-orbit coupling. As elementary anisotropic scattering mechanisms, so far, the quasi-classical skew scattering (first order) and the quantum mechanical (second order) side jump have been proposed. These mechanisms have been investigated in relation to certain (spin) scattering centers, such as spin waves or spin impurities, but apparently other possible spin scattering centers have not been covered as yet.

Fig. 5 shows the longitudinal MR as a function of magnetic field upto 0.6 T at RT. The initial large change in the MR occurs in the low field which is accompanied by growth of magnetic domain parallel to the direction of the magnetic field. Once the magnetic saturation is achieved there is no domain motion as it has assumed a single domain. The only contribution to the electrical resistivity and the MR comes at this stage is from the conduction electron scattering due to the collision between themselves and the electron mean free-path is much longer in this stage. The MR varies from 0 to 8 % with the increase of V content and also with the applied magnetic field.

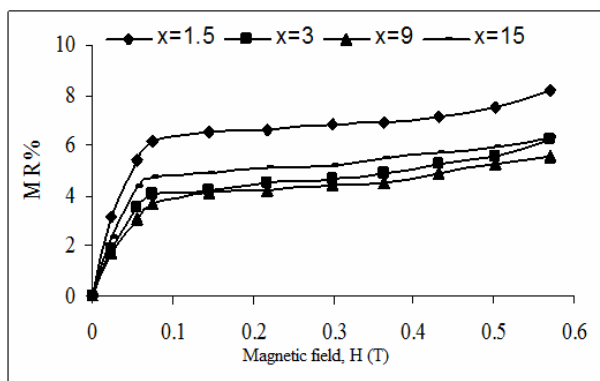


Figure 5. MR% as a function of magnetic field .

3. 3. Magnetization

When a magnetic field is applied, the magnetic domains easily align and the magnetization saturates for relatively low applied fields. Magnetization as a function of magnetic field at RT is shown in Fig. 6. From this study it is found that the role of V is similar to addition of a non-magnetic

solute in a magnetic alloy which is depicted in the magnetization curves of all the studied samples. The values of saturation magnetization for $x=1.5, 3, 9$ and 15 are $139.7, 126.3, 77.4$ and 40.2 emu/gm respectively which agrees with the literature value [35]. Thus the measured values of Bohr magneton for $x=1.5, 3, 9$ and 15 are $1.19, 1.08, 0.66$ and 0.33 per Fe atom respectively.

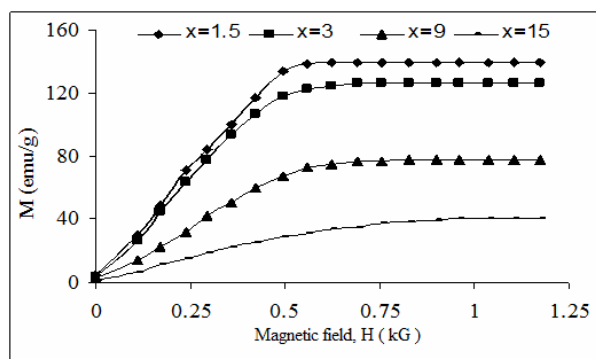


Figure 6. Magnetization as a function of magnetic field.

3.4. Impedance

Fig. 7(a-b) shows the impedance and the corresponding phase angle at different frequencies. From Fig. 7(a) we observed that the impedance remained constant upto 10^6 Hz afterwards it began to increase with the increases of frequency and then reach a maximum value of 110Ω at 10^8 Hz. Similarly, phase angle increases with the increase of frequency as shown in Fig. 7(b). Upto 10^6 Hz the impedance is purely resistance since the phase angle is almost zero. After 10^6 Hz the reactance part of the complex impedance starts to dominate over the resistance part. At 10^8 Hz the phase angle is close to 90° with increasing trend, indicating that at higher frequency it acts as a pure inductor.

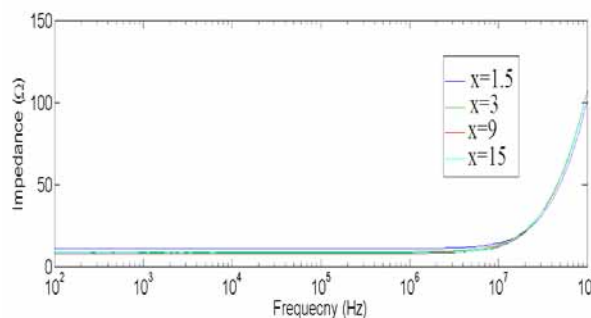


Figure 7(a). Impedance as a function of frequency .

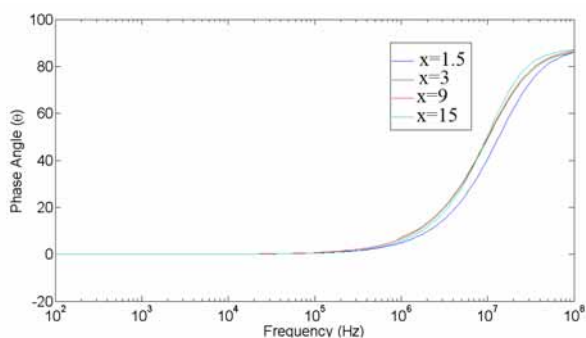


Figure 7(b). Phase angle as a function of frequency .

3.5. DTA and TG

DTA of examined glassy alloys in as cast state allowed determining crystallization temperature. A two stage crystallization process was observed for these alloys. Crystallization peak values in DTA measurement of different samples are shown in Fig. 8(a) and also tabulated in Table 1. The first peak rises sharply, which indicates spontaneous

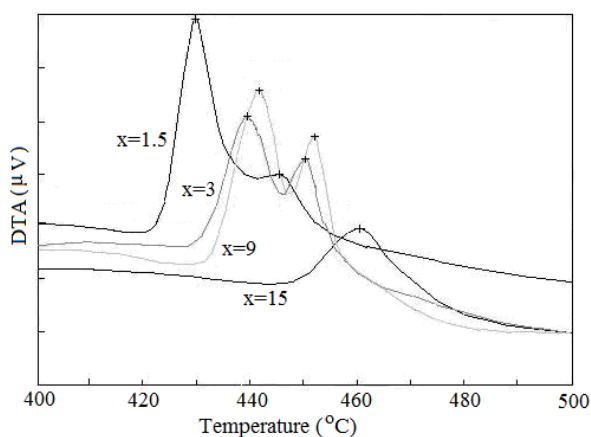


Figure 8 (a). DTA as a function of temperature

Table 1. Peak values in DTA measurement and TG% at 800 °C.

Samples, x	1 st Peak (°C)	2 nd Peak (°C)	TG% at 800 (°C)
1.5	429.6	445.9	104.5
3	439.6	449.5	105.8
9	440.2	451.3	102.4
15	460.8	---	104.2

nucleation and grain growth, which suggests that the delay between nucleation and grain growth is

very small. The second peak corresponds to crystallization of the residual amorphous phase. The crystallization temperature and the broadness of the peaks increased with the increase of V content. The two stage crystallization had been also observed of other measurements of amorphous alloys [36]. Fig. 8 (b) of TG measurement shows that the mass is slightly enhanced for all samples. Changes of TG% at 800 °C of different samples are also shown in Table 1. Passively, as the temperature is increased the micro voids which formed during the growth process of the ribbon during melt spinning are gradually eliminated. Then at higher temperatures Fe and V ions absorb oxygen from the environment and hence the mass could be slightly enhanced. This mass gain had been also founded in TG measurement of different compositions of $(Fe_{100-x}Mn_x)_{75}P_{15}C_{10}$ amorphous ribbons [34]. The volume/grain increases also with the increase of the V content because the ionic radius of V (1.92 Å) is larger than the ionic radius of Fe (1.72 Å).

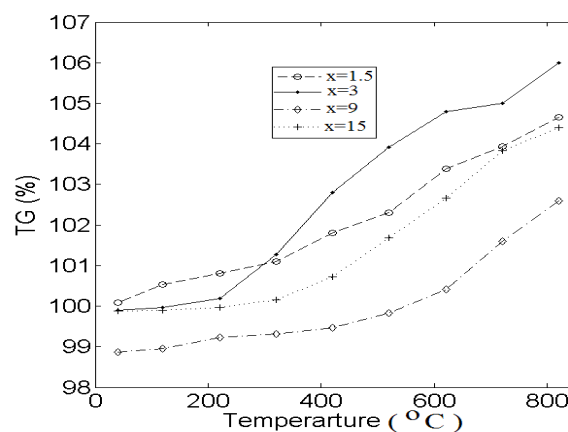


Figure 8 (b). TG% as a function of temperature .

4. Conclusions

Transport, magnetic and thermal measurements were done on a semi-amorphous Fe-V-P-C series ribbons. Positive TCR for the samples of x=1.5, 3 and negative TCR for the samples of x=9, 15 were observed in the measurement. The resistivity remained constant upto 680 K, 710 K, 715 K and 730K for x=1.5, 3, 9 and 15 respectively and then decreased sharply with the increased of temperature. Anomalous Hall effect was observed in the Hall resistivity measurement. MR varied from 0 to 8% with the applied magnetic field and also with the V content. The values of saturation magnetization were 139.7, 126.3, 77.4 and 40.2 emu/gm for x=1.5, 3, 9 and

15 respectively. Upto 10^6 Hz the impedance acts as a resistor while at 10^8 Hz it acts as an inductor. A two stage crystallization process was observed by DTA measurement. TG showed that mass is slightly enhanced for all samples with the increase of temperature.

Acknowledgements

The authors would like to express their thanks to Professor K. Bärner, Department of Physics, University of Göttingen, Germany for the preparation of the samples and his valuable discussions regarding the results. International Programme in the Physical Sciences (IPPS), Uppsala University, Sweden is thankfully acknowledged for its support.

References

- [1] H. Chiriac and T. A. Ovari, *Prog. Mater. Sci.* **40** (1996) 333.
- [2] J. M. Garcia, A. Asenjo, D. Garcia, C. Prados and M. Vazquez, *J. Non-Cryst. Sol.* **287** (2001) 55.
- [3] P. Vojtanik, *J. Magn. Magn. Mater.* **304** (2006) 159.
- [4] R. Nowosielski and R. Babilas, *Mater. Manuf. Engg.* **20** (2007) 487.
- [5] D. Szewieczek, J. Tyrlík-Held and S. Lesz, *J. Achiev. Mater. Manuf. Engg.* **24** (2007) 87.
- [6] A. Inoue, A. Makino and T. Mizushima, *J. Magn. Magn. Mater.* **215-216** (2000) 246.
- [7] R. B. Schwarz, T. D. Shen, U. Harms and T. Lillo, *J. Magn. Magn. Mater.* **283** (2004) 223.
- [8] K. Heinemann and K. Barner, *Appl. Phys. Lett.* **50** (1986) 1284.
- [9] P. J. Cote and L. V. Meisel, *Glassy Metals*, eds. H. J. Guntherodt and H. Beck, Springer Verlag, Berlin (1981) p. 141.
- [10] A. K. Sinha, *J. Appl. Phys.* **42** (1971) 338.
- [11] S. N. Kaul, W. Kettler and Rosenberg, *Phys. Rev. B* **33** (1986) 4987.
- [12] S. N. Kaul, *Phys. Rev. B* **20** (1979) 5122.
- [13] A. Erle and K. Barner, *J. Magn. Magn. Mat.* **74** (1988) 225.
- [14] S. U. Jen and S. M. Yang, *J. Appl. Phys.* **63** (1988) 4303.
- [15] L. Berger and G. Bergman, *The Hall effect and its application*, eds. C. L. Chien and C. R. Westgate, Plenum Press, New York (1979) p. 55.
- [16] J. H. Mooij, *Phys. Status Solidi A* **17** (1973) 521.
- [17] P. W. Anderson, *Phys. Rev.* **109** (1958) 1492.
- [18] J. Mizia and G. Gorski, *Models of itinerant ordering in crystals: An introduction*, Elsevier Science Publishing Company (2007) p. 131.
- [19] I. Vincze and I. A. Campbell, *J. Phys. F: Met. Phys.* **3** (1973) 647.
- [20] A. T. Aldred, *Int. J. Magn.* **2** (1972) 223.
- [21] G. K. Wertheim, V. Jacarrino, J. H. Wernick and D. N. E. Buchanan, *Phys. Rev. Lett.* **12** (1964) 24.
- [22] A. M. Van der Kraan, D. B. Mooij and K. H. J. Buschow, *Phys. Stat. Solidi B* **88** (1972) 566.
- [23] N. Hamada and H. Miwa, *Prog. Theor. Phys.* **59** (1978) 1045.
- [24] N. Hamada, *J. Phys. Soc. Jpn.* **50** (1981) 77.
- [25] V. L. Moruzzi and P. M. Marcus, *Phys. Rev. B* **45** (1992) 2934.
- [26] A. Paja and K. Kulakowski, *J. Phys. F: Met. Phys.* **9** (1979) 1613.
- [27] U. Mizutani, *Introduction to the electron theory of metals*, Cambridge University Press (2003) p. 418.
- [28] M. Kamruzzamana, I. Z. Rahman and M. A. Rahman, *J. Mater. Proc. Tech.* **119** (2001) 312.
- [29] B. Kaviraj and S. K. Ghatak, *J. Mater. Proc. Tech.* **202** (2008) 119.
- [30] R. Nowosielski, R. Babilas, P. Ochinn and Z. Stoklosa, *Archiv. Mater. Sci. Engg.* **30** (2008) 13.
- [31] A. L. Greer, *Acta Metall.* **30** (1982) 171.
- [32] A. Pratap, K.G. Raval, A. Gupta and S. K. Kulkarni, *Bull. Mater. Sci.* **23** (2000) 185.
- [33] R. C. Budhani, T. C. Goel and K. L. Chopra, *Bull. Mater. Sci.* **4** (1982) 549.
- [34] M. Kamruzzaman, M. Phil. Thesis, BUET, (2010).
- [35] C. C. Tsuei and H. Lilienthal, *Phys. Rev. B* **13** (1976) 4900.
- [36] P. K. Rastogi and P. Duwez, *J. Non-cryst. Sol.* **5** (1970) 1.